

# Structural Characterization on the Gel to Liquid-Crystal Phase Transition of Fully Hydrated DSPC and DSPE Bilayers

Shan-Shan Qin and Zhi-Wu Yu\*

Key Lab of Bioorganic Phosphorous Chemistry & Chemical Biology (Ministry of Education), Department of Chemistry, Tsinghua University, Beijing 100084, P. R. China

Yang-Xin Yu

Department of Chemical Engineering, Tsinghua University, Beijing 100084, P. R. China

Received: October 4, 2008; Revised Manuscript Received: April 28, 2009

The structural properties of fully hydrated distearoylphosphatidylcholine (DSPC) and distearoylphosphatidylethanolamine (DSPE) bilayers near the main phase transition were investigated using molecular dynamics simulations on the basis of a united-atom model. Although largely similar in their molecular structures, the two lipids were found with different molecular packing modes at temperatures below the phase transition. For DSPC, three packing modes, namely, cross-tilt, partially interdigitated, and “mixed” gel phases, were observed, while, for DSPE, the lipid tails were almost perpendicular to the lipid surface. Above the main transition temperature, both lipid bilayers transformed into a disordered liquid-crystal phase with marked greater area per lipid and gauche % of the acyl chains and smaller bilayer thickness and order parameter, in comparison with the gel phase. The transformation process of liquid-crystal to gel phase was proved to experience the nucleation and growth stages in a hexagonal manner. The electron density profiles of some major components of both lipid bilayers at various temperatures have been calculated, and the results reveal that both lipid bilayers have less interdigitation around the main transition temperature.

## 1. Introduction

Phospholipids are a family of amphiphiles with one polar head and two hydrocarbon tails of various length and saturation. Hydrated lipid bilayers have been the subject of great interest both for their intriguing thermodynamic properties and as models of biological membranes.<sup>1</sup> They mainly have three lamellar forms when dispersed in water or aqueous solutions: crystal phase, gel phase, and liquid-crystal phase.<sup>2</sup> Transitions between these phases have not only close biological relevance but also physical chemistry importance. Various computer simulation methods have been used to investigate the phase behavior of model membranes, including Monte Carlo simulation, stochastic dynamics, the continuum electrostatics method, mean field theory, and atomistic and coarse grained molecular dynamics (MD) simulations (for reviews, see refs 3–7). Particularly, the coarse grained (CG) molecular dynamics method has been widely applied to study lipid phase properties, for its ability to deal with large sizes and time scales which are not within reach of full atomic molecular dynamics simulations.

The coarse grained (CG) molecular dynamics method was applied to lipid systems by Smit et al. as early as 1990.<sup>8</sup> A decade later, Marrink et al. developed the MARTINI force field,<sup>9</sup> which was proved to reproduce a variety of structural, dynamic, and thermodynamic properties of lipid membranes on a semi-quantitative level.<sup>9</sup> Using the force field, Marrink and Mark first studied the spontaneous aggregation of a concentrated solution of dipalmitoylphosphatidylcholine (DPPC) molecules in water.<sup>10</sup> Later, they elucidated the complete transition pathway from a multilamellar to an inverted hexagonal phase in near-atomic

detail with the same method.<sup>11</sup> Almost at the same time, Stevens showed that DPPC bilayers have tilted lipid chains at low temperatures and indicated a large hysteresis in the area per lipid and bilayer thickness in heating and cooling cycles of the lipid bilayer.<sup>12</sup> Then, Marrink et al. reported that formation of a gel phase in coarse grained lipid bilayers proceeded via a nucleation and growth mechanism.<sup>13</sup> Also, de Vries et al. performed a detailed MD study of the phase behavior of DPPC and concluded that rippled bilayers consisted of two domains of different length and orientation which were connected by a kink.<sup>14</sup>

Since coarse grained models usually take several carbon atoms and the connected hydrogen atoms as one particle, they are short in describing more subtle structural properties of bilayers. To solve the problem, the united-atom model, which only treats CH<sub>3</sub>, CH<sub>2</sub>, and CH as coarse grains, has been used. On the basis of united-atom models, Heller et al.<sup>15</sup> performed MD simulations of lipid bilayers and analyzed various properties of the bilayers in both the gel and liquid-crystal states. Zubrzycki et al.<sup>16</sup> simulated a fully hydrated DMPC in the liquid crystalline phase at 303.15 K and proved that the area per lipid molecule and electron density files were comparable with X-ray diffraction results. Recently, Leekumjorn and Sum<sup>17</sup> simulated the transition process of DPPC and DPPE from the gel phase to the liquid-crystal phase; they calculated the cross area per lipid, the distance between P atoms from the upper and lower leaflet of a bilayer, the chain tilt, the order parameter, and the trans–gauche percentage during the phase transition process. Later, they performed a similar simulation on POPC and POPE bilayers and gave a full description of the structural information of the gel phase, liquid-crystal phase, and near phase transition state.<sup>18</sup> There have also been studies on the phase behavior of mixed

\* To whom correspondence should be addressed. E-mail: yuzhw@tsinghua.edu.cn.

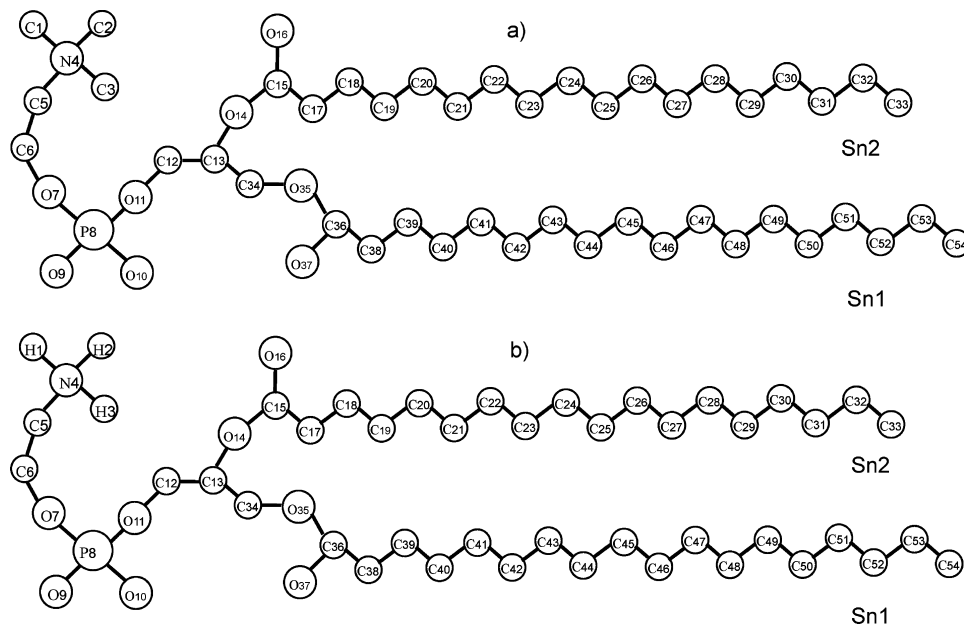


**Figure 1.** Molecular structures and assigned sequence of atoms for (a) DSPC and (b) DSPE.

lipid systems using both coarse grained and united-atom molecular dynamics methods.<sup>19–21</sup>

Despite these reports, atomic MD simulations of phospholipid phase transitions are still rare. Phase transitions of lipids with 18 carbons or longer saturated acyl tails have not been investigated yet. In order to deepen our understanding on the molecular details of lipid phase behaviors and, at the same time, to test the validity of the existing lipid force field on describing the phase behavior of lipids with long saturated chains, we have carried out simulations of two representative lipids: DSPC and DSPE bilayers.

## 2. Simulation Details

Structural properties of distearoylphosphatidylcholine (DSPC) and distearoylphosphatidylethanolamine (DSPE) around the main phase transition temperatures have been investigated using computer simulation. Figure 1 shows the structures of the two lipids. All of the CH<sub>3</sub>, CH<sub>2</sub>, and CH groups have been treated as united atoms, and hydrogen atoms in the amino group of DSPE were considered explicitly due to their capability to form hydrogen bonds. These groups or atoms are labeled in the molecular structures. The simulation included 128 lipids, 64 in the upper leaflet and 64 in the lower leaflet, and the membrane is parallel to the *xy* plane. Periodic boundary conditions in *x*, *y*, and *z* directions were used. To attenuate the influence of the image bilayer, 46 water molecules per lipid were included. Both scanning and fixed temperature simulations were performed. For DSPC, in the scanning temperature simulation, we first raised the temperature from 250 to 370 K and then annealed back to 250 K at a scanning rate of 2 K/ns. The initial structures for heating (at 250 K) and cooling (at 370 K) simulations were both well-equilibrated. We also performed fixed temperature simulations from 250 to 360 K, 10 K apart, and several more temperatures near the phase transition point, to get the well-equilibrated structural information at different temperatures. The initial structures for these simulations were obtained by heating to 370 K, incubating for 150 ns, and then cooling back to the target temperatures at an annealing rate of 2 K/ns. Similar simulations were also carried out for DSPE with the temperature ranging from 270 to 390 K. The initial structures for heating

and cooling simulations were also well-equilibrated structures at 270 and 390 K, and those for fixed temperature simulations were obtained by heating to 390 K, incubating for 100 ns, and then cooling back to the target temperatures. All of the fixed temperature simulations were more than 150 ns, and only the data of the last 40 ns were used for analysis. They are well-equilibrated data.

For DSPC and DSPE, the bonded parameters were downloaded from Peter Tieleman's Web site<sup>22</sup> and the Ryckaert–Belleman potential was used as the torsion potential of the lipid hydrocarbon chains.<sup>23</sup> For nonbonded parameters, we used values extracted from Berger et al.<sup>24</sup> for lipid tails and OPLS values for head groups,<sup>25,26</sup> and the partial atomic charges were obtained from Chiu et al.<sup>27</sup> For water molecules, the SPC model<sup>28</sup> was used with the settle algorithm to constrain bonds and angles.<sup>29</sup>

The force field adapted in this work was originally developed for simulating lipid bilayers at the liquid-crystal state.<sup>24</sup> Later, it was proved to be capable of representing gel phase properties of DPPC and DPPE bilayers.<sup>17</sup> Therefore, we used this force field to simulate DSPC and DSPE bilayers at both liquid-crystal and gel phase states in this work. In order to ensure the statistic reliability, we performed a series of heating and cooling scans of each lipid bilayer system starting from previously equilibrated structures with different conformations and velocities, and the results were consistent with each other.

All of the simulations were carried out in the *NPT* ensemble, at a constant pressure of 1 bar and various temperatures. The time step was 4 fs for all simulations, and the pair list for computing nonbonded pair forces was updated every 10 steps with a list-cutoff of 0.9 nm. The Coulomb and van der Waals interactions were computed using the cutoff algorithm, and the cutoff radius for both Coulomb and van der Waals interactions was 0.9 nm. The long-range electrostatic interaction was corrected using the PME method,<sup>30,31</sup> with a maximum spacing for the FFT grid of 0.12 nm and an interpolation order of 4. The weak coupling scheme of Berendsen and co-workers<sup>32,33</sup> was used for both temperature and pressure control, with a temperature coupling time constant of 0.1 ps. For pressure coupling, we used the anisotropic coupling type, in which the

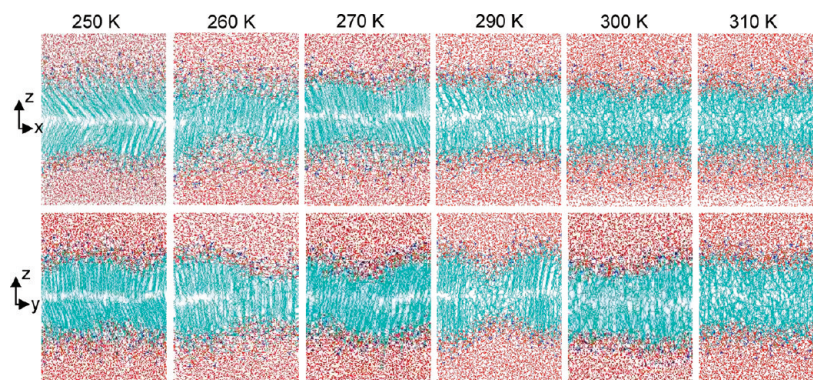


**Figure 2.** Snapshots of equilibrium DSPC configurations at various temperatures in  $xz$  and  $yz$  planes.

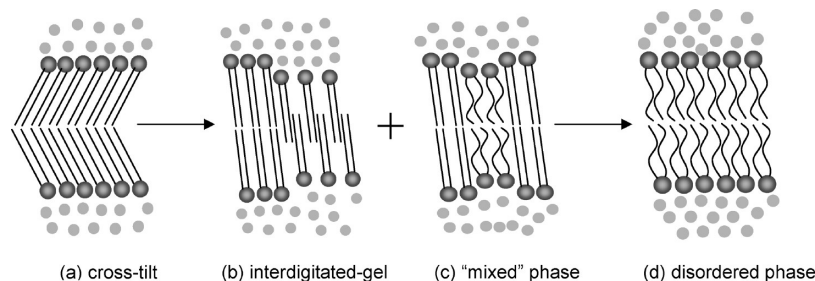


**Figure 3.** Schematic of DSPC tail alignments. The two arrows indicate the transitions from lamellar gel to ripple gel and then to lamellar liquid-crystal phase.

$x$ ,  $y$ , and  $z$  directions of the simulation box could be varied independently, with a coupling time constant of 2.0 ps and a compressibility of  $4.6 \times 10^{-6}$ /bar.<sup>17,18,34</sup> The trajectory was collected every 4 ps, and all of the simulations were performed with the Gromacs 3.3.1 package<sup>35,36</sup> in parallel under a Windows Compute Cluster Server.

### 3. Results and Discussion

#### 3.1. General Features of the Phase Transition Process.

The aim of this study is to better understand the main phase transition of DSPC and DSPE bilayers through characterizing the structural properties of the assembled lipid molecules at gel and liquid-crystal states. In order to get a general impression of the phase transition process of the two lipids, their equilibrated structures were obtained first at various temperatures.

Figure 2 shows the snapshots of DSPC bilayer structures at various fixed temperatures. To present the structures more clearly, views on both  $xz$  and  $yz$  planes are displayed. We can see from Figure 2 that at 250 K the arrangement of lipid molecules is at a very ordered state with a tilt angle to the bilayer normal. This is the typical lamellar gel phase of phosphatidylcholines ( $L_{\beta}$ ).<sup>2</sup> Interestingly, molecules at this state are cross-tilted, as illustrated by Figure 3a. At 260 K, the packing mode changes into the partially interdigitated-tilt gel state, as illustrated by Figure 3b, which appears as a ripple phase ( $P_{\beta}$ ),<sup>2</sup> with part of the bilayers overlapped and no disordered domain existed in this situation. When the temperature is between 270 and 300 K, two distinct domains are observed. The first domain consists of lipids that are fully stretched, and there is no overlap between lipid tails from the adjacent lipids. This is referred to as the "ordered" domain. Molecules in this domain are still tilt. The second domain is identified as the disordered arrangement of the lipid tails and is referred to as the "disordered" domain. Both ordered and disordered domains exist in DSPC bilayers, resulting in a difference in bilayer thickness, as illustrated by Figure 3c. This type of lipid alignment is the typical ripple phase

( $P_{\beta}$ ) in lecithin by de Vries et al.<sup>14</sup> The lipid tails become fully random at 300 K, indicating a typical lamellar liquid-crystal phase ( $L_{\alpha}$ ), as illustrated by Figure 3d. This change in the packing manner of the lipid tails corresponds to the phase transformation first from  $L_{\beta}$  to  $P_{\beta}$  and then from  $P_{\beta}$  to  $L_{\alpha}$ . From Figures 2 and 3, we find that the P–P distance experiences an obvious increase at 270 K accompanied by a decrease in the area per lipid, which corresponds to the change from cross-tilt packing manner to tilt packing manner.

Figure 4 shows a series of snapshots of DSPE at various temperatures. Just like DSPC, views on both  $xz$  and  $yz$  planes are displayed. Only the ordered phase with tilt tails can be observed in the figure at temperatures between 270 and 330 K. All lipid tails are tightly packed, and the ripple phase is absent. At temperatures above 330 K, the lipid tails become fully random, indicating that it is a typical lamellar liquid-crystal phase.

Regarding the formation of the ripple phase in lipid bilayers, three conditions have been summarized in our previous work: (1) intrinsic steric repulsion between the lipid head groups that arises from the relatively large size and weak binding of the headgroup; (2) mildly weak packing on the acyl chains of lipid molecules; and (3) relatively weak interactions between the head groups.<sup>37</sup> In comparison with phosphatidylcholine molecules, phosphatidylethanolamine molecules have stronger head–head interactions (hydrogen bonding) and relatively smaller head groups, giving less or no intrinsic steric repulsion in the headgroup region of the bilayer. The DSPE bilayer, therefore, shows no ripple phase.

**3.2. Determination of Transition Temperatures.** Two main structure properties considered here are the area per lipid and the lipid bilayer thickness, which are sensitive to phase states and thus can be used to characterize the main transition temperature. The area per lipid was obtained from the cross-sectional area of the simulation box (plane perpendicular to the  $z$  axis) divided by the number of lipids, i.e., 64. The thickness

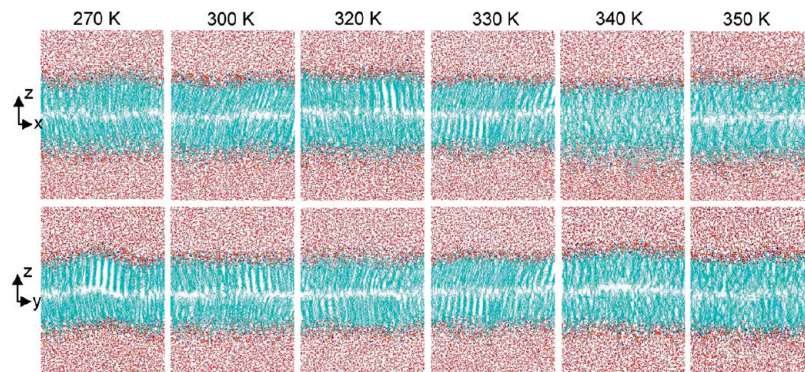


**Figure 4.** Snapshots of equilibrium DSPE configurations at various temperatures in  $xz$  and  $yz$  planes.

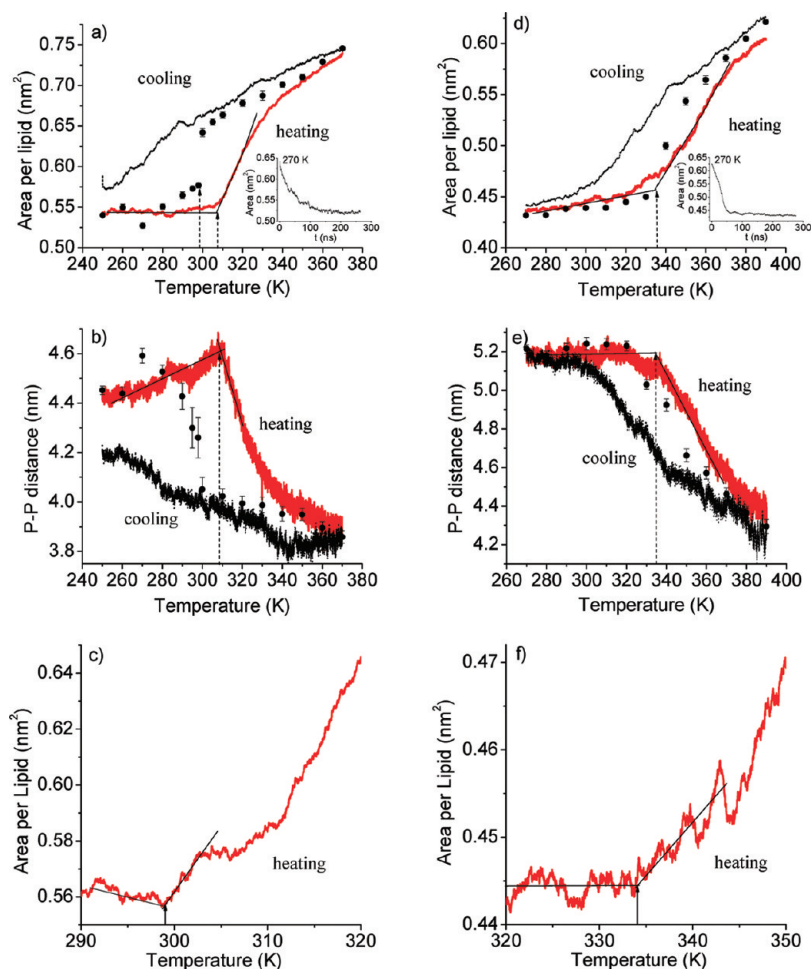


**Figure 5.** Area per lipid and P–P distance of DSPC (a, b, c) and DSPE (d, e, f) obtained from heating–cooling cycle and fixed temperature simulations. Red solid and dotted lines correspond to the heating and cooling scans, respectively, dots stand for fixed temperature simulations, and error bars are estimated standard deviation. The scanning rate of temperature is 2 K/ns (a, b, d, e) and 1 K/ns (c, f).

of the bilayer was calculated by subtracting the average position of phosphorus atoms in the lower leaflet from that in the upper leaflet. We put the variation of area per lipid with respect to time at 270 K in the subwindow of Figure 5a and Figure 5d as a representative to validate the system equilibrium.

Figure 5a and b depict, respectively, the area per lipid and thickness of DSPC bilayers. The heating and cooling processes are expressed in solid and dotted lines, respectively. Upon heating, the average area of a lipid molecule keeps nearly constant until 308 K, followed by an abrupt increase, as shown in Figure 5a. This turning point, however, cannot be regarded as the phase transition temperature, which will be explained later. The corresponding temperature dependence of bilayer

thickness gives a consistent abrupt change at 308 K. The P–P distance increases significantly with increasing temperature from 250 to 308 K, resulting from the changes on the tilt angle of lipid molecules. Above the phase transition temperature, the lipid bilayer thickness drops much more significantly due to the disordering of the lipid acyl chains. Upon cooling, both the area and bilayer thickness curves cannot reproduce the results on heating, and there is no obvious phase transition turning point. This is due to the well-known hysteresis effect, a predominant characteristic of any material that undergoes a first-order phase transition mechanism.<sup>38–40</sup>

Simulations in the same way were carried out on DSPE, and the results are shown in Figure 5d and e, with the solid and

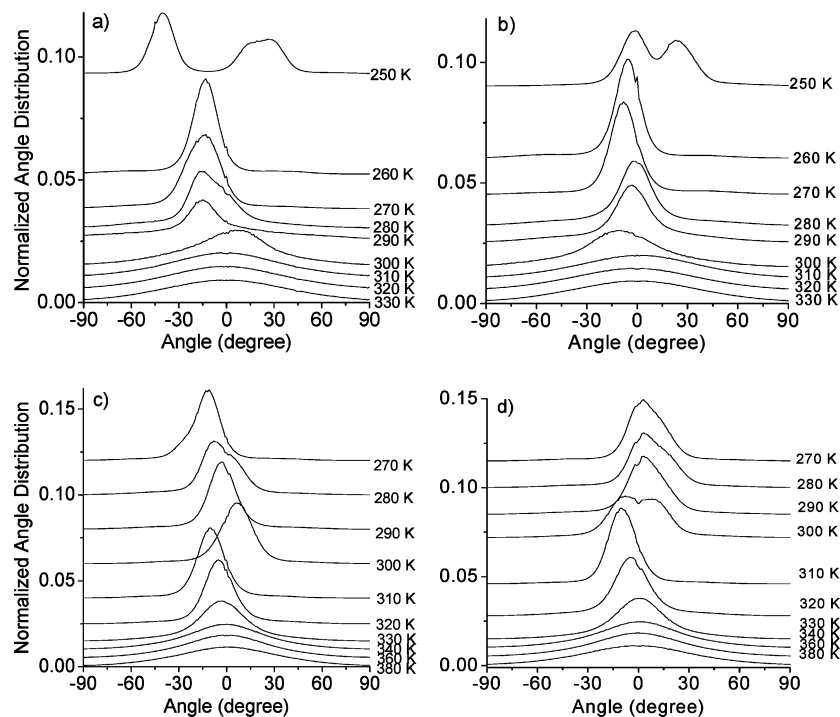


**Figure 6.** Tilt angle distribution of DSPC (a, b) and DSPE (c, d) at various temperatures in  $xz$  (a, c) and  $yz$  (b, d) planes. Baselines have been up-shifted.

dotted curves standing for heating and cooling processes, respectively. A main transition temperature of 335 K can be obtained. The general features of the temperature-dependence properties of DSPE are quite like those of DSPC, except that the area increases slightly and the bilayer thickness keeps almost constant as the temperature is increased to the main phase transition temperature.

Different from the results of scanning temperature simulation, a drastic increase in the lipid area in the fixed temperature simulations is seen at about 299 K, as shown in Figure 5a. Since the heating scan begins with the well equilibrated structure at 250 K, which is in “cross-tilt” packing mode, and equilibrated structures at the temperature range from 260 to 290 K are all another type of “tilt” packing mode, the change of tail packing mode may require slower heating scan in reflecting phase transition temperature. In order to minimize this kind of influence, we calculated another heating scan beginning with a well equilibrated structure at 290 K with a scanning rate of 1 K/ns, and the inflection of this curve was found at about 299 K (Figure 5c), which is in good accordance with the phase transition temperature determined from the fixed temperature simulations. It is worthwhile to mention that the scanning rate 2 K/ns might not be sufficient for bilayers to become completely equilibrated at different temperatures, so the structures at various steps in annealing simulations are not equilibrated ones. As for the temperatures from 250 to 290 K, the area per lipid from the fixed temperature simulations stands quite close to the curve of the heating scan; this is due to the fact that the area per lipid from the fixed temperature simulations at this temperature range does not change much. From 300 to 370 K, the area per lipid from the fixed temperature simulations changes almost linearly with temperature, a feature qualitatively in agreement with that for DPPC reported by Leekumjorn and Sum.<sup>17</sup> Since the cooling scan begins from the equilibrated structure at 370 K, the structures in the first part of the cooling scan are very close to the initial structure in the liquid-crystal phase. Thus, it is not a

surprise that areas per lipid from the fixed temperature simulations from 300 to 370 K locate close to the curve of the cooling scan.

For DSPE, as shown in Figure 5d, we can see from fixed temperature simulations that the area per lipid increases drastically from 330 to 340 K and the inflection point determined by the heating curve locates at about 335 K. The phase transition temperatures determined by heating scan and fixed temperature simulations show good consistency here, unlike the case for DSPC. For comparison, we also calculated the heating scan from 320 to 350 K at a heating rate of 1 K/ns, and the result is shown in Figure 5f. The phase transition temperature determined from Figure 5f is approximately 334 K. Probably this is due to the needlessness of rearrangement of lipid tails during the phase transition process of DSPE.

The bilayer thickness is also calculated for different temperatures and compared with annealing simulations. As shown in Figure 5b, in the heating scan of DSPC, the P–P distance of DSPC increases quite notably as the temperature is increased from 250 to 308 K, which is related to a change in the alignment of lipid tails from the cross-tilt to tilt phase. Above 308 K, the P–P distance of DSPC decreases drastically with increasing temperature, corresponding to the phase transition from an ordered state to a disordered one. From the fixed temperature simulations shown in Figure 5b, one can find there is a drastic decrease of P–P distance between 298 and 300 K, consistent with the transition temperature determined by the area per lipid from the fixed temperature simulations in Figure 5a. We can also see an abrupt increase of P–P distance at 270 K, which represents the change from the “cross-tilt” packing mode to the “tilt” packing mode and accords well with the minimum area per lipid in the fixed temperature simulation at 270 K. For DSPE shown in Figure 5e, no such behavior of increasing P–P distance before the phase transition occurs, since the lipid tails are closely packed without a notable change of tilt angle at low temperatures. There is also an inflection point at 335 K determined from

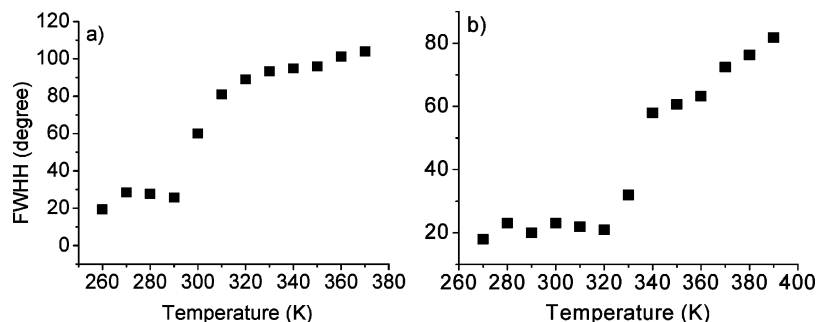


**Figure 7.** Full width at half height (FWHH) obtained from the tilt angle distribution shown in Figure 6. The results are for DSPC (a) and DSPE (b) at various temperatures.

the heating scan, indicating that it is the phase transition temperature for DSPE. Further analysis of the lipid tail packing mode will be discussed in the next section.

**3.3. Properties at Fixed Temperatures.** To characterize and quantify the changes of bilayer structure near the phase transition temperature for DSPC and DSPE, we analyzed a number of properties including area per lipid, bilayer thickness, lipid tail tilt angle, lipid tail order parameter, lipid tail trans-gauche isomerization, and density distribution of carbon atoms in lipid tails. These properties were obtained from the ensemble average of the trajectories over the simulation results of the last 40 ns for each system at respective fixed temperatures. The stability of each system was monitored by the average area per lipid.

The simulation results of lipid area and bilayer thickness have been shown in Figure 5 and described in section 3.2. Now let us make a comparison with the results determined experimentally. The surface area per lipid and the lipid repeating distance for DSPC at 333 K measured by small angle neutron scattering are  $0.6478 \pm 0.0046 \text{ nm}^2$  and 4.15 nm, respectively,<sup>41</sup> while the calculated values for DSPC in our present work are 0.68  $\text{nm}^2$  and 3.98 nm at 330 K. In the case of DSPE, Majewski measured an area per lipid of 0.40  $\text{nm}^2$  at 294 K,<sup>42</sup> while the calculated value in our study was 0.44  $\text{nm}^2$  at 290 K. Liu determined a mean hydrophobic length of DSPE at the gel phase of 4.47 nm,<sup>43</sup> while our calculated value was 4.50 nm. The simulated and experimental values are generally in good agreement.

To further verify the structural transformation of DSPC and DSPE during the phase transition, we analyzed the lipid tail tilt angle with respect to the bilayer normal at various fixed temperatures. To calculate tilt angles, we defined the vector between each  $n$ th and  $(n+2)$ th carbons in the lipid tail as a segment, and projected the segment onto  $xz$  and  $yz$  planes following the work of Leekumjorn and Sum.<sup>17</sup> We then calculated the acute angles between the projection and the  $z$

axis, and defined the sign of the angle to be the sign of the projection's  $x$  or  $y$  value. Figure 6 shows the normalized tilt angle distributions of DSPC and DSPE at various temperatures in  $xz$  and  $yz$  planes. As shown in the figure, there are three distinct angle distribution patterns, indicating different structural alignment of the lipid molecules. The double peak refers to the cross-tilted lipid arrangement, while the single sharp peak implies that the lipid tails are predominantly tilted to one direction which corresponds to the tilted lipid arrangement. The wide distribution centered at around  $0^\circ$  indicates that the lipid tails are disordered. Clearly, the sharp-peak patterns are from the gel state lipid dispersions and the broad-peak pattern is from the liquid-crystal phase. To further illustrate the relation between the lipid tail alignments and the phase transformation, we analyzed the full width at half height (FWHH) of the peak maximum at various temperatures, without considering the curves with double peaks. The results are summarized in Figure 7 for both DSPC and DSPE systems. We can see from the figure that there is a sudden jump in the FWHH between 290 and 300 K for DSPC and a sudden increase between 330 and 340 K for DSPE. These are the temperature ranges when the ordered alignment of the lipids melts, in good agreement with the phase transition temperatures determined from other parameters.

The deuterium order parameter<sup>44</sup> has also been evaluated around the phase transitions of the two lipids. The order parameter is expressed by the formula

$$S_{\text{CD}} = 1/2 \langle 3 \cos^2 \theta_{\text{CD}} - 1 \rangle \quad (1)$$

where  $\theta_{\text{CD}}$  is the angle between the carbon-hydrogen bond and the bilayer normal in the acyl chains. It is a parameter to illustrate the level of order of hydrocarbon chains. It has been reported that the alignment of the lipid tails in a gel state is more ordered (higher  $|S_{\text{CD}}|$  value) than those in a liquid

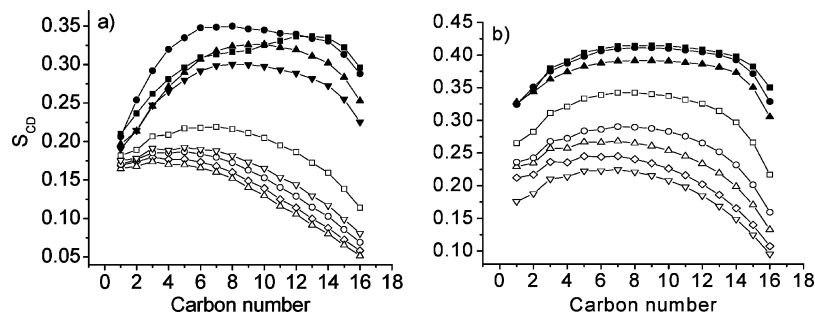


**Figure 8.** Deuterium order parameter of DSPC (a) and DSPE (b) at various temperatures. For DSPC: 260 K (■), 270 K (●), 280 K (▲), 290 K (▼), 300 K (□), 310 K (▽), 330 K (○), 350 K (◇), 360 K (△). For DSPE: 270 K (■), 300 K (●), 330 K (▲), 340 K (□), 350 K (○), 360 K (△), 370 K (◇), 380 K (▽).

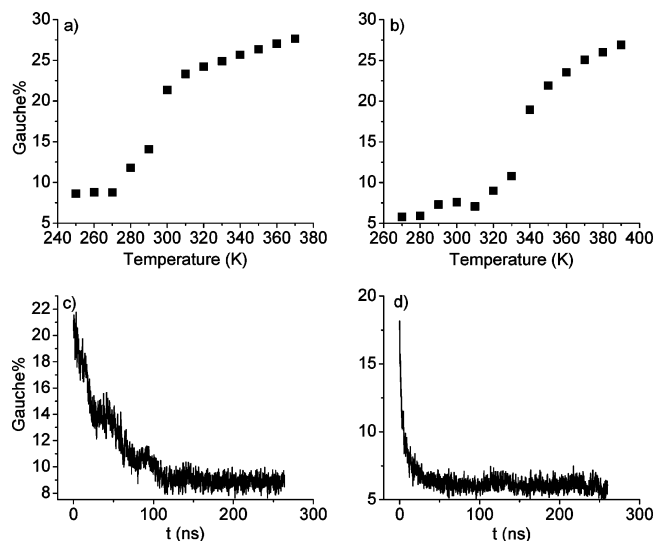


**Figure 9.** Average gauche % of the acyl chains of DSPC (a) and DSPE (b) at various temperatures. Trans fraction vs time for DSPC (c) and DSPE (d) cooled instantaneously to 270 K.

crystalline state.<sup>44</sup> Figure 8 shows the  $S_{CD}$  parameter of Sn2 tails for DSPC and DSPE at various temperatures. We can see from the figure that between 260 and 290 K the DSPC bilayer has a high  $S_{CD}$  parameter, which indicates a well aligned lipid tail packing mode. Above 300 K, the ordering of the lipid tails decreases with the increase of temperature, due to the increasing random movement of the lipid tails at high temperature.<sup>44</sup> We can also see from the figure that the  $S_{CD}$  parameter has a marked decrease from 290 to 300 K, which characterizes the phase transition from an ordered state to a disordered state. For DSPE, the  $S_{CD}$  parameter decreases suddenly from 330 to 340 K, indicating a main phase transition.

The hydrocarbon trans–gauche isomerization property around the main phase transition has also been calculated in the present work. Here, we defined the gauche configuration as dihedrals of four successive carbon atoms in the lipid tails between  $-120$  and  $120^\circ$ ,<sup>45</sup> and the calculated gauche % for DSPC and DSPE are shown in Figure 9a and b as a function of temperature. As can be seen from the figure, for DSPC below 270 K, i.e., at the gel state, the gauche % is less than 10%. This is explained as follows: at low temperatures, the trans conformations are preferred because they are energetically more favorable for the lipids in the bilayer arrangement. With the increase of temperature, the gauche conformers increase gradually until 300 K, where a drastic change is observed. Above the phase transition temperature, the gauche % becomes greater than 20%, due to the fact that the carbon atoms in the lipid tails are less restricted to move. In the case of DSPE, the gauche % at 270–280 K is even less than 6%, indicating a very ordered arrangement of the acyl chains. The marked increase of the gauche conformers occurs at a temperature between 330 and 340 K, which refers to the main phase transition from the gel phase to the liquid-crystal phase. The gauche % for DSPC and DSPE are at the same level in their liquid-crystal states.

Since the trans fraction can be regarded as a hallmark of gel phase formation,<sup>46</sup> we plotted its variation with respect to time to describe the transformation process from the liquid-crystal phase into the gel phase. Furthermore, we analyzed the nucleation process during gel phase formation. The simulations started from equilibrated liquid-crystal configurations (at  $T = 310$  K for DSPC and  $T = 350$  K for DSPE) which were then cooled instantaneously to 270 K. Figure 9c and d show the

variation of trans fraction with respect to time for DSPC and DSPE bilayers at 270 K. We can see from the graphs that the time needed for the slope of the trans fraction curve of DSPC to become near zero is 120 ns and the time for DSPE is 25 ns, which indicates that DSPE bilayers are easier to transform into the gel phase than DSPC bilayers. Earlier research has shown that this process is extremely slow and depends on nucleation, followed by a faster progression and then a slow step to get rid of defects.<sup>13</sup> In order to find the nucleated sites, a Voronoi analysis was performed on the trajectories using the Triangle program<sup>47</sup> to calculate the lipid coordination numbers. The Voronoi cells were computed using the positions of the C24 and C45 atoms in Sn2 and Sn1 tails (see Figure 1) in each of the monolayers, that is to consider each lipid tail as a single component. Two conditions must be satisfied for a lipid tail to be considered as in gel phase. First, each carbon site must have exactly six neighbors, and second, all of these neighbors must lie within a cutoff distance of  $D_{cut} = 0.7$  nm for DSPC and  $D_{cut} = 0.6$  nm for DSPE molecules.  $D_{cut}$  is determined by the distance of the first minimum value of the radial pair distribution function  $g(r)$  of the carbon sites in the equilibrated gel phase.

Although, due to the small system size and the use of a rectangular box (as the lipid packing should become hexagonal), different stages of nucleation are difficult to exhibit distinctly, we still find out that the number of molecules that form nucleated sites increases with time. Figure 10a shows the number of nucleated sites in the upper leaflet at different time steps (1 ns per step). We may find that the nucleated number fluctuates drastically from time to time but is inclined to increase as a whole. As shown in the picture, the DSPE bilayer has more nucleated sites formed in the first tens of nanoseconds. This may be due to the fact that DSPE molecules are less fluid than DSPC at the same temperature and thus more favorable for the formation of nucleated sites. Figure 10b and c show some snapshots representing different stages of gel phase formation, and we can see that when transforming from the liquid-crystal phase into the gel phase, the nucleated sites in both bilayers form and grow in hexagonal shapes.

We further analyzed the electron density distributions of some major components as well as the whole lipid molecules in both lipid monolayers at various temperatures. The results are shown in Figure 11. Let us examine the general features of the electron density profiles first. For all 12 profiles, the electron densities are lowest at the bilayer center where methyl groups locate, forming a trough, and are highest at the interfacial region, where the heaviest atoms phosphorus reside. These are in good agreement with the experimentally determined electron density profiles of various lipid bilayers including our previous works.<sup>37,48,49</sup> The profiles are smooth and almost perfectly symmetric at high temperatures when lipids are at the liquid-crystal state, indicating fast moving of the molecules in the bilayers. Different from this, multiple peaks can be seen on the density profiles at low temperatures, suggesting much restricted movement of the molecules in the gel phase.

Other than the electron density profiles of the whole lipid bilayers, profiles of water, phosphate group  $PO_4$ , methylene, and methyl groups in lipid acyl chains of DSPC and DSPE bilayers are also plotted in the figures. Several features can be seen from the figures. For DSPC at 250 K, the phosphate group has a narrow and sharp distribution, Water can penetrate about 1.0 nm into the lipid acyl tail region. The electron density profile of the methylene groups has a very low value ( $47 \text{ e/nm}^3$ ) at the bilayer center, and that of the terminal methyl group has a narrow distribution spreading about 1 nm around the bilayer

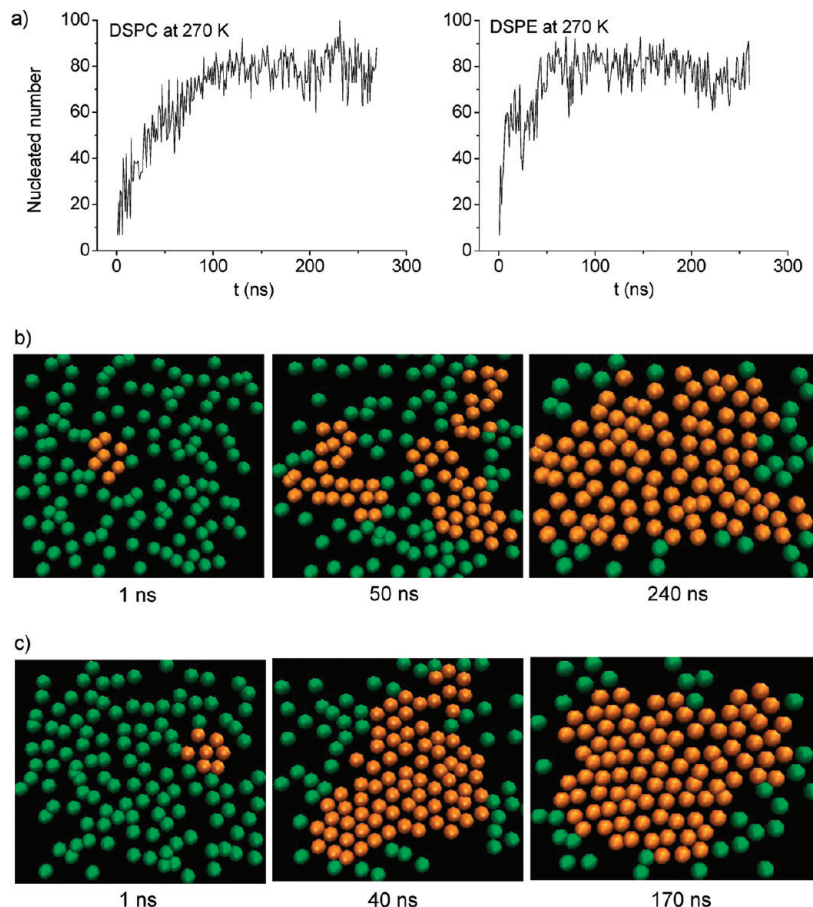


**Figure 10.** (a) Number of nucleated molecules in the upper leaflet at different time steps (1 ns per step). Carbon sites in the upper leaflet for DSPC (b) and DSPE (c) during the transformation process from the liquid-crystal phase into the gel phase. Nucleated sites: orange. Sites not nucleated: green.

center, indicating that interdigitation occurs between the lipids in the upper and lower leaflets. This is in accordance with the cross-tilt lamellar gel phase displayed in Figure 2, where mild overlap is observed in the snapshots at 250 K.

At 270 K, the electron density profile of the phosphate group becomes wider distributed with multiple peaks, which indicates that phosphorus atoms locate in different depths with respect to the bilayer normal. This feature accords well with the “mixed” phase nature of the DSPC bilayer. As shown in Figure 2, the mixed phase includes molecular packing of both ordered and disordered domains. We may also notice that at 270 K the electron density profile of methylene groups in the bilayer center has a value of 121 ( $e/\text{nm}^3$ ), which is greater than that at 250 K, and the electron density distribution of the terminal methyl group spreads about 2 nm, indicating a higher level of interdigitation compared with the situation at 250 K.

Upon further increase of the temperature to 290 and 300 K, the values of the distribution curves of the methylene group at the bilayer center decrease drastically. This is explained as a consequence that around the phase transition temperature the lipid tails tend to get out of the interdigitation state to change their packing mode, and when DSPC molecules are at the liquid-crystal phase, interdigitation of methylene groups becomes obvious again because of the random moving mode of the lipid tails.

For DSPE, the electron density of the methylene group has a value of 78 ( $e/\text{nm}^3$ ) at the bilayer center at 270 K. This value decreases to 60, 25, and 34 ( $e/\text{nm}^3$ ) at 300, 330, and 340 K, respectively. Similar to the temperature-dependent feature of

DSPC, this is explained as the fact that DSPE acyl tails tend to get interdigitated at low temperatures to have lower energy but try to decrease the interdigitation level when the temperature becomes higher. After the main phase transition occurs, the DSPE acyl tails stay in a random moving mode and interdigitation becomes significant again. We may also notice that, below 340 K, the density profiles of the phosphate group have narrow distributions without multiple peaks, indicating a gel state absent from the “mixed” phase. Above 340 K, the density profiles become smoother and more diffused, showing that the lipids are now in the liquid-crystal state.

#### 4. Conclusion Remarks

MD simulations were performed to investigate the structural properties of DSPC and DSPE bilayers. We performed two sets of simulations: scanning simulations (both heating and cooling) and fixed temperature simulations. The scanning simulations showed an obvious phase transition point from liquid ordered phase to liquid disordered phase with small hysteresis upon cooling. We calculated the area per lipid and the distance between the average position of 64 phosphorus atoms in the upper leaflet and 64 phosphorus atoms in the lower leaflet to trace the phase transition behavior of lipid bilayers. Both parameters show different slopes before and after the main transition temperature, and the inflections represent the phase transition point. The calculated main transition temperatures were 299 and 335 K for DSPC and DSPE, respectively, which were obviously smaller than the experimental values of 327 and 347 K.

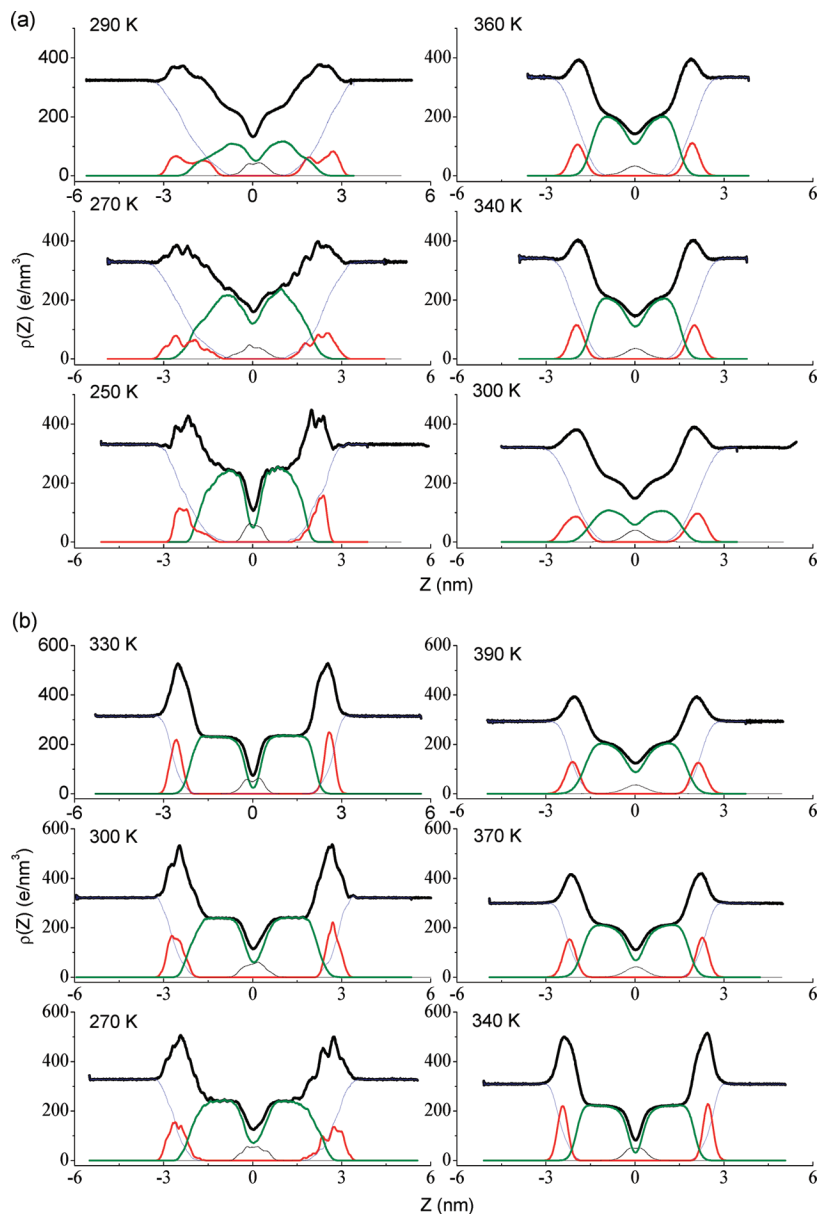


**Figure 11.** Electron density profiles of some major components at different temperatures for (a) DSPC, (b) DSPE. Water: blue line. Phosphate group: red line. Methylene group: green line. Methyl group: thin black line. Whole lipid bilayers: bold black line.

In the fixed temperature simulations, we calculated a series of parameters to characterize the structural changes of the lipid bilayers near the main transition temperatures. For DSPC, we found that the phase transition process can be divided into three steps according to the packing modes of lipid tails: first from cross-tilted packing mode to tilted packing mode, then to “mixed” alignment, and at last to randomly disordered existence. At low temperatures (250–260 K), the lipid bilayer stays in the ordered gel phase and the hydrocarbon tail changes from cross-tilt to tilt packing mode. At higher temperatures (270–300 K), the lipid bilayer keeps its alignment in tilted mode and becomes more disordered with increasing temperature. Above the main phase transition temperature, the lipid tails stay in a much more disordered state, which can be described by the increase of gauche %, FWHH, and the decrease of  $S_{CD}$ . The simulation also indicates that the trans conformer still dominates even at the liquid-crystal phase, with less than 30% gauche conformers.

The phase transition for DSPE is similar to that of DSPC, except for the absence of the “mixed” phase due to its smaller

head groups. This is also reflected in the smaller area per lipid and tilt angles, and is in accordance with the less marked rearrangement of lipid tails and the gradual decrease of bilayer thickness near the transition point in the scanning simulation. Around the main phase transition temperature, cooperative structural changes are observed with the decrease in the ordering of the lipid tails and the increase in the gauche % conformation and FWHH. Above the main transition temperature, the DSPE bilayer can be characterized by lipid tails able to move in a more random manner, resulting in an increase in the gauche % conformation and decrease in the order parameter.

We also studied the transformation from the liquid-crystal phase to the gel phase and found that both lipid bilayers went through the nucleation and growth stages in a hexagonal manner. At last, we calculated the electron density profiles of some major components of both lipid bilayers at various temperatures and the results revealed that both lipid bilayers had less interdigitation around the main transition temperature.

In summary, the phase transition of DSPC and DSPE model bilayers can be characterized by cooperative changes of area

per lipid, bilayer thickness,  $S_{CD}$  parameter, gauche %, and FWHM of tilt angle distribution. Both bilayers transform from the liquid-crystal phase into the gel phase, experiencing the nucleation and growth stages in a hexagonal manner. Also, both lipid bilayers have less interdigitation around the main transition temperature. Our study provides insights into the structural changes that DSPC and DSPE bilayers experience during the gel to liquid-crystal phase transition. The structural parameters we calculated can help in the understanding of the mechanism of phase transition of DSPC and DSPE, which may not be easily obtained from experimental measurements.

**Acknowledgment.** This work was supported by grants from the Natural Science Foundation of China (20633080 & 20675046). Y.-X.Y. greatly appreciates the financial support of Specialized Research Fund for the Doctoral Program of Higher Education (No. 20070003099).

## References and Notes

- (1) Cevc, G.; Marsh, D. *Phospholipid Bilayers: Physical Principles and Models*; Wiley-Interscience: New York, 1987.
- (2) Kranenburg, M.; Smit, B. *J. Phys. Chem. B* **2005**, *109*, 6553.
- (3) Pahle, J. *Briefings Bioinf.* **2009**, *10*, 53.
- (4) Marrink, S. J.; de Vries, A. H.; Tieleman, D. P. *Biochim. Biophys. Acta* **2009**, *1788*, 149.
- (5) Venturoli, M.; Sperotto, M. M.; Kranenburg, M.; Smit, B. *Phys. Rep.* **2006**, *437*, 1.
- (6) Nielsen, S. O.; Lopez, C. F.; Srinivas, G.; Klein, M. L. *J. Phys.: Condens. Matter* **2004**, *16*, R481.
- (7) McCullagh, M.; Prytkova, T.; Tonzani, S.; Winter, N. D.; Schatz, G. C. *J. Phys. Chem. B* **2008**, *112*, 10388.
- (8) Smit, B.; Hilbers, P. A. J.; Esselink, K.; Rupert, L. A. M.; van Os, N. M.; Schlijper, A. G. *Nature* **1990**, *348*, 624.
- (9) Marrink, S. J.; de Vries, A. H.; Mark, A. E. *J. Phys. Chem. B* **2004**, *108*, 750.
- (10) Marrink, S. J.; Mark, A. E. *J. Am. Chem. Soc.* **2003**, *125*, 15233.
- (11) Marrink, S. J.; Mark, A. E. *Biophys. J.* **2004**, *87*, 3894.
- (12) Stevens, M. J. *J. Chem. Phys.* **2004**, *121*, 11942.
- (13) Marrink, S. J.; Risselada, J.; Mark, A. E. *Chem. Phys. Lipids* **2005**, *135*, 223.
- (14) de Vries, A. H.; Yefimov, S.; Mark, A. E.; Marrink, S. J. *Proc. Natl. Acad. Sci. U.S.A.* **2005**, *102*, 5392.
- (15) Heller, H.; Schaefer, M.; Schulten, K. *J. Phys. Chem.* **1993**, *97*, 8343.
- (16) Zubrzycki, I. Z.; Xu, Y.; Madrid, M.; Tang, P. *J. Chem. Phys.* **2000**, *112*, 3437.
- (17) Leekumjorn, S.; Sum, A. K. *Biochim. Biophys. Acta* **2007**, *1768*, 354.
- (18) Leekumjorn, S.; Sum, A. K. *J. Phys. Chem. B* **2007**, *111*, 6026.
- (19) de Joannis, J.; Jiang, F. Y.; Kindt, J. T. *Langmuir* **2006**, *22*, 998.
- (20) de Joannis, J.; Jiang, Y.; Yin, F. C.; Kindt, J. T. *J. Phys. Chem. B* **2006**, *110*, 25875.
- (21) Coppock, P. S.; Kindt, J. T. *Langmuir* **2009**, *25*, 352.
- (22) [http://moose.bio.ucalgary.ca/index.php?page=Structures\\_and\\_Topologies](http://moose.bio.ucalgary.ca/index.php?page=Structures_and_Topologies).
- (23) Ryckaert, J. P.; Bellemans, A. *Chem. Phys. Lett.* **1975**, *30*, 123.
- (24) Berger, O.; Edholm, O.; Jähnig, F. *Biophys. J.* **1997**, *72*, 2002.
- (25) Jorgensen, W. L.; Tirado-Rives, J. *J. Am. Chem. Soc.* **1988**, *110*, 1657.
- (26) Essex, J. W.; Hann, M. M.; Richards, W. G. *Philos. Trans. R. Soc. London, Ser. B* **1994**, *344*, 239.
- (27) Chiu, S. W.; Clark, M.; Balaji, V.; Subramaniam, S.; Scott, H. L.; Jakobsson, E. *Biophys. J.* **1995**, *69*, 1230.
- (28) Berendsen, H. J. C.; Postma, J. P. M.; van Gunsteren, W. F.; Hermans, J. *Intermolecular Forces*; Reidel: Dordrecht, The Netherlands, 1981.
- (29) Miyamoto, S.; Kollman, P. A. *J. Comput. Chem.* **1992**, *13*, 952.
- (30) Darden, T.; York, D.; Pedersen, L. *J. Chem. Phys.* **1993**, *98*, 10089.
- (31) Essmann, U.; Perera, L.; Berkowitz, M. L.; Darden, T.; Lee, H.; Pedersen, L. G. *J. Chem. Phys.* **1995**, *103*, 8577.
- (32) Berendsen, H. J. C. Transport properties computed by linear response through weak coupling to a bath. In *Computer Simulations in Material Science*; Meyer, M., Pontikis, V., Eds.; Kluwer: Dordrecht, The Netherlands, 1991.
- (33) Berendsen, H. J. C.; Postma, J. P. M.; DiNola, A.; Haak, J. R. *J. Chem. Phys.* **1984**, *81*, 3684.
- (34) Leekumjorn, S.; Sum, A. K. *Biophys. J.* **2006**, *90*, 3951.
- (35) Berendsen, H. J. C.; van der Spoel, D.; van Drunen, R. *Comput. Phys. Commun.* **1995**, *91*, 43.
- (36) Lindahl, E.; Hess, B.; van der Spoel, D. *J. Mol. Model.* **2001**, *7*, 306.
- (37) Yu, Z. W.; Quinn, P. J. *Biophys. J.* **1995**, *69*, 1456.
- (38) Suurkuusk, J.; Lentz, B. R.; Barenholz, Y.; Biltonen, R. L.; Thompson, T. E. *Biochemistry* **1976**, *15*, 1393.
- (39) Davis, J. H. *Biophys. J.* **1979**, *27*, 339.
- (40) Huang, C. H.; Li, S. S. *Biochim. Biophys. Acta* **1999**, *1422*, 273.
- (41) Balgavy, P.; Dubnickova, M.; Kucerka, N.; Kiselev, M. A.; Yaradaikin, S. P.; Uhrikova, D. *Biochim. Biophys. Acta* **2001**, *1512*, 40.
- (42) Majewski, J.; Kuhl, T. L.; Kjaer, K.; Gerstenberg, M. C.; Al-Nielsen, J.; Israelachvili, J. N.; Smith, G. S. *J. Am. Chem. Soc.* **1998**, *120*, 1469.
- (43) Liu, F.; Lewis, R. N.; A, H.; Hodges, R. S.; McElhaney, R. N. *Biophys. J.* **2004**, *87*, 2470.
- (44) Lu, D. L.; Vavasour, I.; Morrow, M. R. *Biophys. J.* **1995**, *68*, 574.
- (45) Tu, K.; Tobias, D. J.; Blasie, J. K.; Klein, M. L. *Biophys. J.* **1996**, *70*, 595.
- (46) Egberts, E.; Marrink, S. J.; Berendsen, H. J. C. *Eur. Biophys. J.* **1994**, *22*, 423.
- (47) Shewchuk, J. R. Triangle: Engineering a 2D Quality Mesh Generator and Delaunay Triangulator. In *Applied Computational Geometry: Towards Geometric Engineering*; Lin, M. C., Manocha, D., Eds.; Springer-Verlag: Berlin, 1996; Vol. 1148, p 203.
- (48) Yu, Z. W.; Quinn, P. J. *Biochim. Biophys. Acta* **2000**, *1509*, 440.
- (49) Gao, W. Y.; Chen, L.; Wu, R. G.; Yu, Z. W.; Quinn, P. J. *J. Phys. Chem. B* **2008**, *112*, 8375.